Biosensors and Bioelectronics 126 (2019) 405–411

Contents lists available at ScienceDirect

Biosensors and Bioelectronics

journal homepage: www.elsevier.com/locate/bios

An integrated microfluidic device with solid-phase extraction and graphene oxide quantum dot array for highly sensitive and multiplex detection of trace metal ions

Minsu Park[a], Tae Seok Seo[b,*]

[a] Department of Chemical and Biomolecular Engineering, Korea Advanced Institute of Science and Technology (KAIST), 291 Daehak-ro, Yuseong-gu, Daejeon 34141, Republic of Korea

[b] Department of Chemical Engineering, College of Engineering, Kyung Hee University, 1 Seochon-dong, Giheung-gu, Yongin-si, Gyeonggi-do 17104, Republic of Korea

ARTICLE INFO

Keywords:
Microdevice
Solid-phase extraction
Graphene oxide quantum dot
DNA aptamer
Metal ion sensor

ABSTRACT

An integrated microfluidic device, consisting of a solid-phase extraction (SPE) unit for metal ion pretreatment, a micropump, a micromixer, and a detachable graphene oxide quantum dot (GOQD) array chip was constructed for selective and sensitive detection of As^{3+}, Cd^{2+}, and Pb^{2+}. The entire process could be sequentially and automatically completed by actuating a pneumatic micropump. Effect of the pH for metal ion capture and pumping scheme for recovery efficiency were investigated on a chip. The ion As^{3+}, Cd^{2+}, and Pb^{2+} whose concentrations ranged from 10^{-2} μM to 10^{2} μM were successfully recovered with high efficiency over 80%. Monoplex and multiplex detection of As^{3+}, Cd^{2+}, and Pb^{2+} were then executed on a GOQD array chip. The target metal ions were specifically captured on the DNA aptamer linked GOQD array, which results in the fluorescence quenching of GOQD due to the electron transfer from the GOQD to metal ions under the laser irradiation. The proposed integrated SPE-GOQD array based microdevice could perform As^{3+}, Cd^{2+}, and Pb^{2+} detection with detection limits of 5.03 nM, 41.1 nM, and 4.44 nM, respectively. Simultaneous multiplex detection for binary or ternary mixture of As^{3+}, Cd^{2+}, and Pb^{2+} was performed, and the proposed integrated microdevice also showed high recovery values ranging from 83.52% to 128.3% from the environmental samples.

1. Introduction

Despite the cutting-edge science and analytical technologies for analyzing water contaminants, on-site applications for detecting trace level of multiplex heavy metals have still challenges in terms of selectivity, sensitivity, and portability. Lab-on-a-chip (LOC) technology or microfluidics can fulfill these demands due to the advantages of automatic operation, low reagent consumption, and high-throughput capability by integrating functional units on a single wafer (Daw and Finkelstein, 2006). During the past decades, various types of heavy metal detection platforms based on microfluidic technology have been reported such as an on-chip mercury microelectrode for electrochemical detection of Cd^{2+} and Pb^{2+} (Zhu et al., 2005), a microchip for optical fibre based Pb^{2+} detection with the use of fluorescent sensor (Zhao et al., 2009), a polymeric photonic lab-on-a-chip system for Hg^{2+} and Pb^{2+} detection by absorbance change (Ibarlucea et al., 2013), and a biphasic droplet based microfluidic device for Hg^{2+} detection using the fluorescent gated sensory nanoparticles (Bell et al., 2016).

However, most of them lack of studies for real sample pretreatment or preconcentration, which should be accomplished for trace detection prior to practical analysis (Arpa and Bektas, 2006). Besides, the use of expensive metal sources such as gold, and platinum (Zhu et al., 2005) or a costly fluorescent dyes (Zhao et al., 2009) is quite unfavorable in terms of cost effectiveness. Also, they focused only on monoplex detection (Bell et al., 2016), and the microdevice still requires tedious handwork for operation (Ibarlucea et al., 2013). In this regards, an automatically operable and integrated portable system, which is equipped with a sample pretreatment unit and a detection unit on a single microdevice, is of importance for sensitive multiplex detection of trace metal ions.

For selective separation of trace metal ions from a raw aqueous sample, an on-chip solid-phase extraction (SPE) endows many benefits such as fast extraction time, low sample consumption, and easy downsizing (Camel, 2003; Chen et al., 2010; Date et al., 2012). For sensitive metal ion detection using the change of fluorescence signal (Bothra et al., 2017a,b; H. N. Kim et al., 2012; Valeur and Leray, 2000),

* Corresponding author.
E-mail addresses: voltare@kaist.ac.kr (M. Park), seots@khu.ac.kr (T.S. Seo).

https://doi.org/10.1016/j.bios.2018.11.010
Received 6 September 2018; Received in revised form 3 November 2018; Accepted 10 November 2018
Available online 15 November 2018
0956-5663/

graphene quantum dots (GQDs) or graphene oxide quantum dots (GOQDs), the well-known graphene families with nanometers in size, are highly promising (Ananthanarayanan et al., 2014; Ha et al., 2015; Li et al., 2014; Park et al., 2015; Sun et al., 2013; Wang et al., 2014) due to their unique characteristics, for example, water dispersability, facile surface modification, and excellent photoluminescence (Li et al., 2013; Shen et al., 2012; Zheng et al., 2015). Our group has demonstrated the fluorescence (FL) quenching of graphene oxide microarray for detecting DNA hybridization (Liu et al., 2010), pathogen (Jung et al., 2010), and heavy metal ions (Liu et al., 2013). Also, highly sensitive detection for trace Pb^{2+} by combining an off-chip GOQD sensor with an on-chip sample preconcentration has been reported recently (Park et al., 2015).

Herein, we constructed an integrated microfluidic device that is composed of a SPE based sample pretreatment part and a GOQD array chip for highly sensitive and multiplex detection of trace As^{3+}, Cd^{2+}, and Pb^{2+}. By using the proposed microdevice, the target metal ions from the raw aqueous sample could be selectively separated by an on-chip SPE, and then automatically transferred to the DNA aptamer linked GOQD array sensor for quantitative analysis with the detection limit of 5.03 nM, 41.1 nM, and 4.44 nM for As^{3+}, Cd^{2+}, and Pb^{2+}, respectively. We also successfully performed the multiplex detection and environmental sample analysis of As^{3+}, Cd^{2+}, and Pb^{2+} on our microdevice.

2. Materials and methods

2.1. Design and fabrication of an integrated SPE-GOQD array microdevice

First, an integrated microfluidic device, which incorporates a SPE based sample pretreatment system and a detachable GOQD array sensor, was fabricated by a conventional photolithography (Choi et al., 2012; Kim et al., 2016). A detailed fabrication procedure is described in Supplementary Information (Fig. S1). Fig. 1 shows the overall scheme of an integrated SPE-GOQD array microdevice for trace heavy metal detection. The microdevice has an alternate glass (SiO_2)-polydimethylsiloxane (PDMS) hybrid structure, and is composed of two multilayered parts: i) the SPE sample pretreatment unit and ii) a GOQD array sensor unit (Fig. 1A). The former consists of five layers: from top to bottom, a glass manifold, a monolithic PDMS adhesive, a glass microchannel layer, a PDMS chamber, and a top glass wafer. The glass manifold, the monolithic PDMS membrane, and the patterned glass microchannel layer are semi-permanently bonded and operated as a 3-layer microvalve system (Au et al., 2011; Grover et al., 2003) for loading the aqueous sample. The glass microchannel layer has three parallel patterned microfluidic channels and three via holes, which positioned at the end of the channels for transferring the sample to the PDMS chamber layer. The glass microchannel layer, the PDMS chamber, and the top glass wafer are permanently assembled via O_2 plasma treatment to prevent any leakage during SPE. The top glass wafer has an identical micropattern design with a PDMS chamber and a single microchannel with via holes for transferring the metal ion solution to a GOQD array sensor unit. The GOQD array sensor unit is made up of three layers: from top to bottom, a bottom glass wafer, a monolithic PDMS adhesive, and a glass GOQD array chip. The bottom glass wafer has a patterned single microchannel with a Y-shaped micromixer for neutralization of acidic eluent and continuous flow from SPE pretreatment unit to the GOQD array sensor. The disposable GOQD array chip was located at the end of a micromixer channel and was attached to the bottom side of the bottom glass wafer using a monolithic PDMS adhesive. Finally, the two multilayered units were permanently bonded to complete the fabrication. A digital image for the assembled microdevice is shown in Fig. 1B.

2.2. Preparation of a DNA aptamer linked GOQD array chip

First of all, the GOQD was fabricated according to our previous report (Ha et al., 2015). Details of the synthetic procedure and characterization of GOQD are described in Supplementary Information (Section 1.3, and Fig. S2-S3 in Supplementary Information). An amino-modified glass slide was immersed in a 1 M hydrochloric acid (HCl) solution for 3 h to activate the amino group. A PDMS film, which has 8 holes with 1 mm diameter, was attached on glass slide, and 18 μL of a GOQD solution were deposited on the glass slide. The negatively charged GOQD could be bound to the positively charged surface of the activated amino-modified glass via electrostatic interaction. After vigorous washing with deionized water (DI-water), 1 μL of 1-ethyl-3-(3-(dimethylamino)propyl)carbodiimide (EDC) (12 mM), and N-hydroxysulfosuccinimide (sulfo-NHS) (3 mM) in DI-water were dropped on each GOQD array and incubated for 2 h to activate the carboxylic group of GOQD. Next, 0.5 μL of an amino-modified DNA aptamer solution (50 μM) was drop-casted on the GOQD array, and incubated in humid conditions overnight. Finally, after vigorous washing with DI-water to remove non-reacted DNAs, a DNA aptamer conjugated GOQD array was obtained. The DNA-GOQD array sensor can be reused by regenerating the DNA aptamers with treatment of chelators (Li et al., 2010a) or acidic/basic solutions (Okamoto et al., 2009). The circle-shaped GOQD array shows bright green colour upon the laser irradiation with excitation at 488 nm. As-prepared GOQD array chip was semi-permanently attached below the bottom glass layer using a monolithic PDMS membrane.

2.3. On-chip SPE sample pretreatment

First, we performed the SPE sample pretreatment on a chip to separate target metal ions (As^{3+}, Cd^{2+}, and Pb^{2+}) from the aqueous sample. A strong acidic gel-type polystyrene cation exchanger with sulfonic acid functional groups (Amberlite IRN77) was used for the adsorption of As^{3+}, Cd^{2+}, and Pb^{2+}. According to the previous literature (Helfferich, 1962), the ion exchange occurs between the sulfonic acid groups on a divinylbenzene copolymer and metal ions. A detailed specification of Amberlite IRN77 is summarized in Table S1. The resins were loaded by pipetting them into the SPE chamber via the resin inlet on a microdevice. A As^{3+}, Cd^{2+}, and Pb^{2+} containing aqueous solution (1 mL) was injected to the inlet 1, and transferred to the SPE chamber by actuating a micropump (Choi et al., 2012; Y. T. Kim et al., 2012; Park et al., 2015), which is connected to the manifold 1 with a flow rate of 84 μL/min. The injected metal ions were then adsorbed onto the cation exchange resins, and any impurities that are not positively charged were flushed out to the outlet 1 as a waste (i of Fig. 1C). Then, the adsorbed metal ions are eluted by 600 μL of 7% HCl and collected to the outlet 1. The SPE chamber has a weir structure that prevents the leakage of the resins, while the eluted metal ions could be released (ii of Fig. 1C). The total time required for the sample pretreatment is less than 20 min. Each metal ion concentration of an initial sample, a waste, and an eluent was measured by an inductively coupled plasma mass spectrometry (ICP-MS) (PerkinElmer, Waltham, MA, USA) to compare the accuracy of on-chip sample pretreatment. The capture yield (%) of resins was calculated using the concentration difference between the initial solution and the waste solution, and the recovery (%) of SPE on a chip is calculated as 100 times of the quantities of eluted metal ions (g) divided by the quantities of adsorbed metal ions (g). The acidic eluent was neutralized to pH 7 to pH 8 by mixing an equimolecular sodium hydroxide (NaOH) solution in the outlet 1 for on-chip metal ion detection.

2.4. On-chip metal ion detection on the photoluminescent GOQD array chip

To evaluate the sensing capability of on-chip metal ion detection by a photoluminescent GOQD array sensor, three aqueous solutions were prepared. Each solution has different concentration of As^{3+}, Cd^{2+}, and Pb^{2+}, respectively, and were used for the corresponding metal ion specific DNA aptamer linked GOQD array chip for individual detection

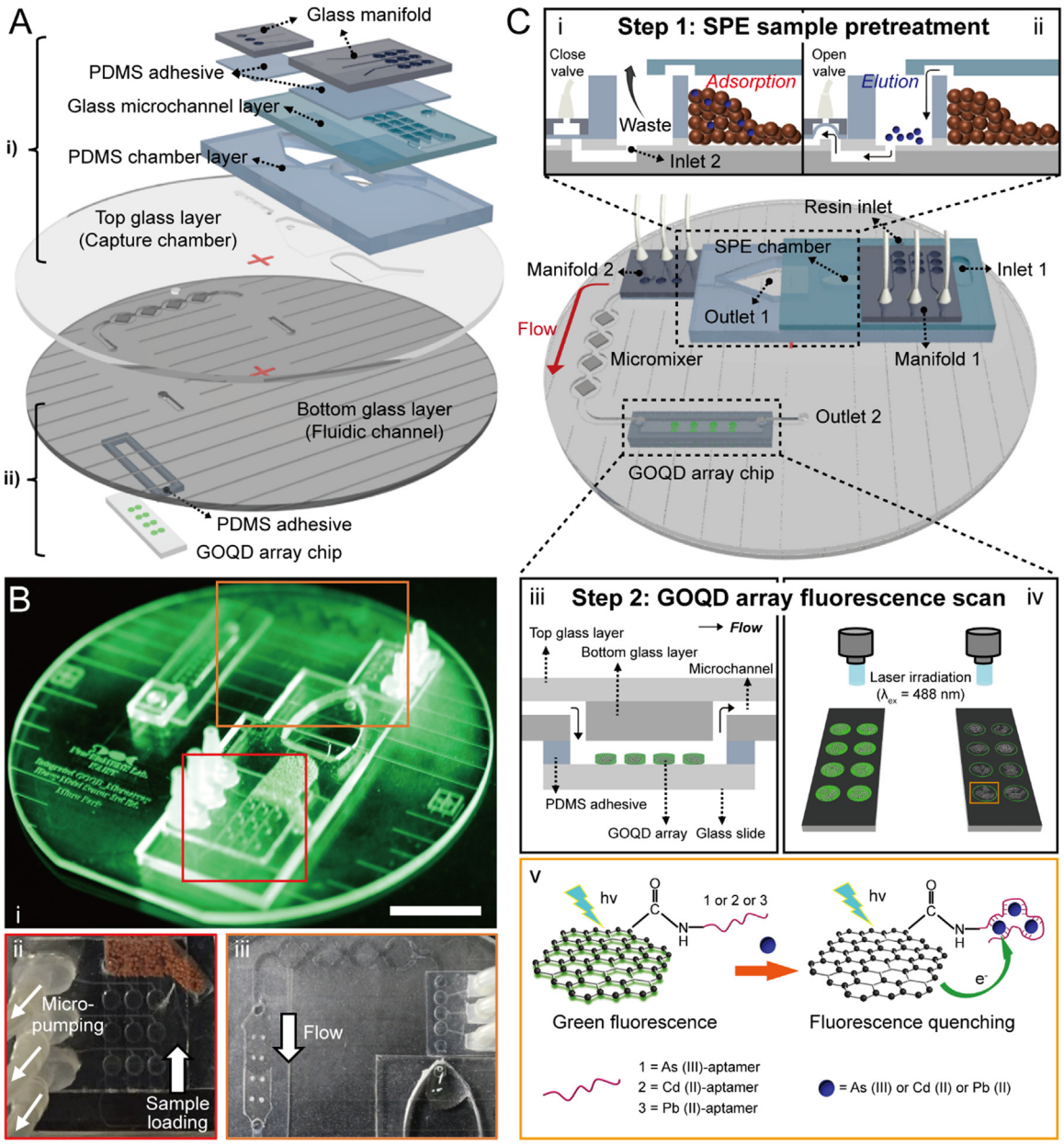

Fig. 1. (A) Structural illustration of a multilayered SPE-GOQD array microdevice. The microdevice is made up of a glass manifold, a monolithic PDMS adhesive, a glass microchannel layer, a PDMS chamber layer, a top glass layer, a bottom glass layer, a monolithic PDMS adhesive, and a glass GOQD array. (B) i) A digital image of an assembled microdevice. Scale bar: 2 cm. ii, iii) Top views of red, and orange boxes in i). White thin arrows indicate three ports on the manifold that connected to external pneumatic pump lines, and white thick arrows represent the direction of a micropump-induced liquid flow. (C) Experimental scheme of on-chip metal ion detection by an integrated SPE-GOQD array microdevice. Step 1 illustrates a sample pretreatment process including i) adsorption and ii) elution of target metal ions by on-chip SPE using cation exchange resins. Brown and blue spheres indicate resins, and metal ions, respectively. Step 2 describes a FL scanning of a GOQD array. iii) Binding process of metal ions on the DNA-GOQD array in a microchamber. iv) FL scanning upon laser irradiation (excitation at 488 nm) for quantitative metal ion analysis. The FL quenching mechanism of a DNA-GOQD sensor under the presence of target metal ions is briefly depicted in v).

(i.e. an As^{3+} solution was used for the As^{3+}-aptamer linked GOQD array chip for As^{3+} detection). The sequence of As^{3+}, Cd^{2+}, and Pb^{2+}-aptamers that were used in this work is shown in Table S2. After the on-chip SPE sample pretreatment, a 100 μL of each metal ion solution was injected to the inlet 2 (i-ii of Fig. 1C). By actuating a micropump that is connected to the manifold 2, the metal ions finally reached to the GOQD array with a flow rate of 71 μL/min via passing through a Y-shaped micromixer channel (Fig. 2C). The injected solution was completely passed through the GOQD array chip (iii of Fig. 1C) during the micropumping for 20 min, and then discharged via the outlet 2. The GOQD array chip was then separated from the microdevice, and washed with DI-water several times. To confirm the specific metal ion binding, high-resolution X-ray photoelectron spectroscopy (XPS) analysis was performed for the DNA aptamer linked GOQD array before and after metal ion processing. The quantitative analysis of metal ions, which were bound to the DNA aptamer linked GOQD array, was performed by measuring the FL intensity of circle-shaped GOQD dots upon the laser irradiation (iv of Fig. 1C). The FL of the GOQD array was quenched upon the capture of metal ions by electron transfer from GOQD to metal ions (v of Fig. 1C). The entire process of the sample loading and transportation was automatically controlled by an in-house LabVIEW program (National Instruments, Austin, TX, USA). The optical measurement was performed with a laser-scanning confocal fluorescence microscope (C1si, Nikon, Japan) using an excitation wavelength of

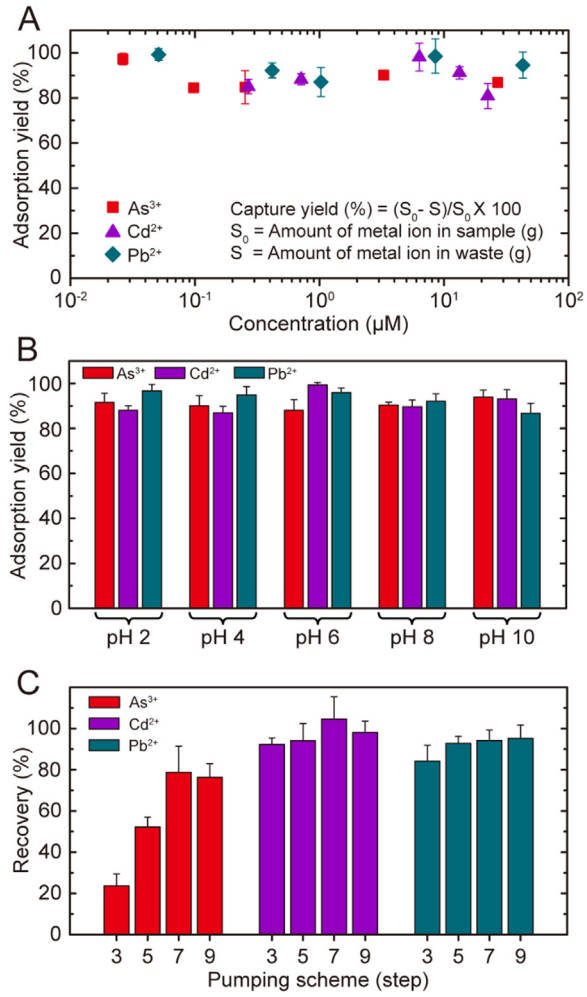

Fig. 2. On-chip As^{3+}, Cd^{2+}, and Pb^{2+} pretreatment of an aqueous sample via SPE. (A, B) Adsorption efficiency of As^{3+}, Cd^{2+}, and Pb^{2+} versus (A) their concentration, and (B) pH value. (C) Recovery yield of As^{3+}, Cd^{2+}, and Pb^{2+} depending on the pumping scheme using 7% HCl as an eluent. All experiments were performed in triplicate.

488 nm from an argon laser. The power intensity from a 10 × Plan Apo objective (NA 0.45) was 3.6 mW. A photo-multiplier tube (PMT) connected with a photon counting unit was used for high-resolution imaging. The fluorescence intensity of the GOQD array was measured by EZ-C1 software (Nikon, Tokyo, Japan) with a gain value of 8.0, and data were obtained with a scanning rate of 5 frames/s.

3. Results and discussion

3.1. On-chip SPE based sample pretreatment

Fig. 2 shows the results of on-chip SPE sample pretreatment for the trace metal ions. First, we evaluated the adsorption performance with variation of metal ion concentration. One mL of a standard aqueous solution that contains certain amount of As^{3+}, Cd^{2+}, and Pb^{2+}, whose concentration range was from 0.026 μM to 42.9 μM, was used. As shown in Fig. 2A, the metal ion adsorption yield of Amberlite IRN77 in a SPE chamber was higher than 80% regardless of metal ion type. In addition to the target metal ions, Cu^{2+}, Fe^{3+}, and Hg^{2+} were also tested as a control experiment. However, the cation exchange resin has little interaction to these metal ions as shown in Fig. S4, which might be attributed to the difference in binding affinity of Amberlite IRN77 toward these metal ions. Although the adsorption efficiency of Hg^{2+} was significant (~28%), As^{3+}, Cd^{2+}, and Pb^{2+} showing higher selectivity would be ideal target ions to be detected in our proposed system. We also investigated the pH-dependent adsorption efficiency of metal ions on a chip. In Fig. 2B, the adsorption efficiency shows high values (> 80%) in the range of pH 2 to pH 10, indicating the resins in a SPE chamber are stable under such acidic change. To elute the captured As^{3+}, Cd^{2+}, and Pb^{2+} from the resins, 600 μL of 7% HCl was used, and the eluent was analyzed by ICP-MS or ICP-AES to estimate recovery yield. We found that the elution process is affected by micropumping scheme as shown in Fig. 2C. The pumping scheme indicates the frequency of microvalve open/close cycles, which induces liquid flow in a typical 3-layer microvalve system (Au et al., 2011; Grover et al., 2003; Lee et al., 2012). For such a reason, the larger pumping scheme leads to the more frequent repetition of microvalve open/close, thereby providing more chances for eluent molecules to contact with adsorbed metal ions (Lee et al., 2012). With a pumping scheme of 3 step, As^{3+} recovery was only 24%, while that of Cd^{2+} and Pb^{2+} were 92.3%, and 84.2%, respectively. The low recovery yield of As^{3+} is attributed to the stronger coulomb interaction between the sulfonate of resins and trivalent As^{3+}. With an increased pumping scheme (5 step: 3 step plus additional two flutter steps, 7 step: 3 step plus additional four flutter steps, a flutter step means additional cycle of microvalve open/close), the As^{3+} recovery yield increased to 52.2% at 5 step and further increased to 78.7% at 7 step, respectively. On the other hand, the recovery yield of Cd^{2+} and Pb^{2+} shows consistently high values (over 92.3% for Cd^{2+}, and over 84.2% for Pb^{2+}) at any pumping scheme. As there was no further increase of recovery yield at 9 step, the 7 step pumping scheme was adopted for metal ion elution process.

3.2. On-chip As^{3+} detection in the As^{3+}-aptamer linked GOQD array

Fig. 3 shows the on-chip monoplex metal ion detection in a GOQD array, which displayed the relative FL intensity ratio (F/F_0; F is the FL intensity of a GOQD array after metal ion processing, and F_0 is that for the pristine GOQD array) of individual metal ion sensor. The As^{3+}-specific single stranded DNA (ssDNA) aptamer was discovered from systematic evolution of ligands by exponential enrichment (SELEX) (Kim et al., 2009), and its application for the colorimetric As^{3+} detection with cationic polymers mediated aggregation of gold nanoparticles was also reported (Wu et al., 2012). As shown in Fig. S5A, the As 3d spectrum after on-chip As^{3+} processing (red line) has a distinct peak at 44.09 eV compare to that of the pristine GOQD array (black line), which indicates the successful binding of As^{3+} on the As^{3+}-aptamer linked GOQD array. Fig. 3A-B represent the As^{3+} detection by the As^{3+}-aptamer linked GOQD array. The F/F_0 of the GOQD array for As^{3+} sensor upon the on-chip As^{3+} processing is shown in Fig. 3A. The F/F_0 value gradually decreased as increasing the As^{3+} concentration, which is consistent with the FL scanning images of a quadruplicate GOQD array (inset images in Fig. 3A). The semilog calibration curve in Fig. 3A shows high linearity in the range from 0.1 μM to 10 mM with the regression coefficient (R^2) of 0.987. The limit of detection (LOD) was 5.03 nM, which was calculated by 3 ×(SD/S). SD is the standard deviation of a blank GOQD array signal, and S is the slope of calibration curve. The LOD value on the proposed microdevice is lower than U.S. Environmental Protection Agency (U.S. EPA) standard for As^{3+} in drinking water (133.48 nM) (EPA, 2009). For selectivity of the GOQD array based As^{3+} sensor, the F/F_0 values were measured in the presence of possibly interfering metal ions (Concentration of all metal ions was 10 mM; Cd^{2+}, Cu^{2+}, Pb^{2+}, Hg^{2+}, Ag^{+}, and Fe^{3+}) under identical experimental conditions. As a negative control (NC), 10 mM of As^{3+} were processed on the pristine GOQD array without As^{3+}-aptamer (blue bar in Fig. 3B). As shown in Fig. 3B, there are no distinguishable FL quenching effect of the As^{3+}-aptamer linked GOQD array toward the non-targeted metal ions with the high F/F_0 values over 0.78, which demonstrated highly selective As^{3+} detection. Moreover, a NC implies that the conjugation of As^{3+}-aptamer on the GOQD array plays a critical role for the specific binding of As^{3+} to trigger electron transfer

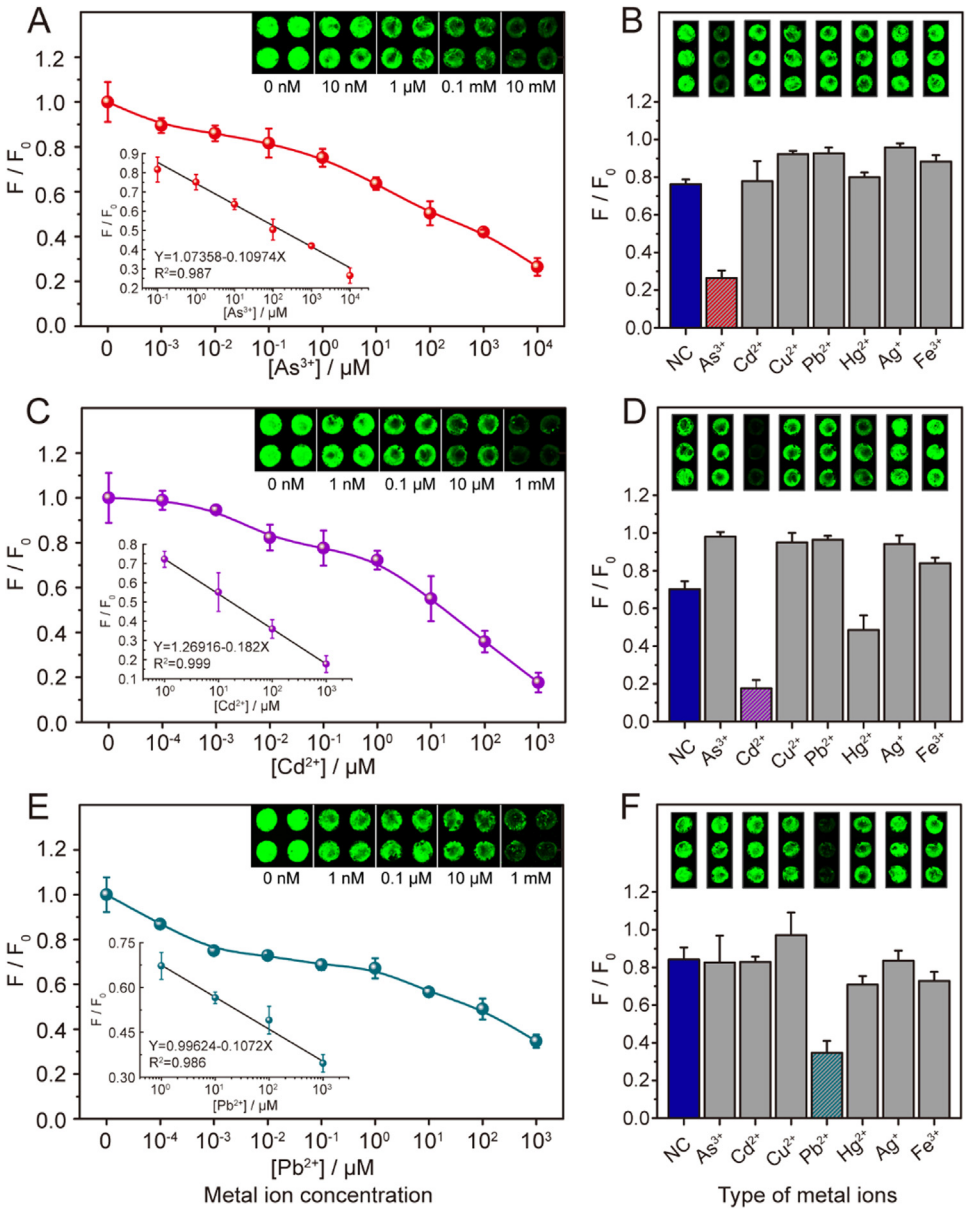

Fig. 3. On-chip As^{3+}, Cd^{2+}, and Pb^{2+} detection by the integrated SPE-GOQD array microdevice. Relative FL intensity ratio (F/F_0) of (A, B) As^{3+}, (C, D) Cd^{2+}, and (E, F) Pb^{2+}-aptamer linked GOQD array. Inset: the FL scanning images of the GOQD array depending on (A, C, E) the concentration, and (B, D, F) the different type of metal ions. (A, C, E) Concentration-dependent monoplex detection of (A) As^{3+}, (C) Cd^{2+}, and (E) Pb^{2+}. The semilog plots represent the linear response for monoplex detection of (inset in A) As^{3+}, (inset in C) Cd^{2+}, and (inset in E) Pb^{2+}, respectively. (B, D, F) Selective detection of (B) As^{3+}, (D) Cd^{2+}, and (F) Pb^{2+} with the other coexisting metal ions. F is the FL intensity in the presence of metal ion, and F_0 is that for the pristine GOQD array. All experiments were performed in triplicate.

mediated FL quenching. These results suggest that the undesirable binding of the non-targeted metal ions on the electron rich regions of GOQD (i.e. carboxyl group) was minor, while the possibilities of electron transfer from GOQD to As^{3+} increased due to the highly specific binding affinity of ssDNA toward the As^{3+}, thereby inducing significant FL reduction of GOQD.

3.3. On-chip Cd^{2+} detection in the Cd^{2+}-aptamer linked GOQD array

Recently, the Cd^{2+}-aptamer was selected by SELEX strategy, and utilized as a recognition element for colorimetric detection of Cd^{2+} (Wu et al., 2014). Since the Cd^{2+} aptamer has newly emerged, the application of aptamer-based Cd^{2+} sensing platform has rarely investigated compare to that of As^{3+} or Pb^{2+}. The Cd 3d spectrum in Fig. S5B after on-chip Cd^{2+} processing (purple line) has two spin-orbit components at 405.51 eV (Cd $3d_{2/5}$) and 412.26 eV (Cd $3d_{2/3}$) compare to that of the pristine GOQD array (black line), which implies that the Cd^{2+} was bound to the Cd^{2+}-aptamer linked GOQD array. Fig. 3C-D show the Cd^{2+} detection in by Cd^{2+}-aptamer linked GOQD array chip. The F/F_0 value of GOQD array for Cd^{2+} sensor upon the on-chip processing of Cd^{2+} is shown in Fig. 3C. The F/F_0 value was gradually decreased as increasing the Cd^{2+} concentration, which is also shown in FL scanning images of quadruplicate GOQD array (inset of Fig. 3C). The semilog calibration curve in Fig. 3C shows high linearity in the range from 1 μM to 1 mM with the regression coefficient (R^2) of 0.999. From the calibration curve, the LOD was calculated as 41.1 nM, which also satisfies U.S. EPA criterion for Cd^{2+} in drinking water (44.48 nM) (EPA, 2009). To evaluate the selective Cd^{2+} sensing capability of the GOQD array sensor, we also measured the F/F_0 values in the presence of possibly interfering metal ions (Concentration of all metal ions was 1 mM; As^{3+}, Cu^{2+}, Pb^{2+}, Hg^{2+}, Ag^{+}, and Fe^{3+}) under identical experimental conditions. As a NC, 1 mM of Cd^{2+} was processed on the pristine GOQD array without Cd^{2+}-aptamer (blue bar in Fig. 3D). In Fig. 3D, Hg^{2+} has some interferences (F/F_0 ~0.51) on the selective Cd^{2+} detection with the quenching efficiency higher than that of a NC (F/F_0 ~0.7), which are ascribed to the strong interaction of Hg^{2+} with the base of thymine (T) within Cd^{2+}-aptamer to form T-Hg^{2+}-T hairpin structure (Ono and Togashi, 2004). Despite of Hg^{2+} interference, reliable Cd^{2+} detection was applicable with significant change of FL intensity (F/F_0 ~0.19) upon 1 mM of Cd^{2+} processing, which was displayed in FL scanning images of the triplicate GOQD array (inset in Fig. 3D). In addition, non-targeted metal ions such as Fe^{3+}, and Hg^{2+}

Table 1
Recovery of As^{3+}, Cd^{2+}, and Pb^{2+} ions in lake water by an on-chip SPE-GOQD array microdevice.

Sample	Type of metal ion	Spiked (μM)[a]	Found (μM)[b]	Recovery (%)
Lake water	As^{3+}	72.3	76.5[c] ± 0.32[d]	105.81
		488.2	481.7 ± 0.8	98.67
	Cd^{2+}	0.0109	0.0114 ± 0.02	104.59
		59.2	69.1 ± 1.63	116.72
	Pb^{2+}	0.0841	0.1079 ± 0.03	128.30
		0.625	0.522 ± 0.087	83.52

[a] The concentration of a spiked sample was measured by ICP-MS or ICP-AES.
[b] The concentration of a spike sample measured by the on-chip SPE-GOQD array microdevice.
[c] Mean values for triplicate measurements.
[d] Standard deviation of triplicate measurements.

could be removed in advance by on-chip SPE pretreatment (Fig. S4).

3.4. On-chip Pb^{2+} detection in the Pb^{2+}-aptamer linked GOQD array

A previous literature demonstrated the colorimetric and chemiluminescence sensor for Pb^{2+} detection based on the binding property of Pb^{2+} to the G-quadruplex DNA structure (Li et al., 2010b). The Pb 4 f XPS spectrum in Fig. S5C after on-chip Pb^{2+} processing (dark cyan line) also shows the two characteristic peaks at 138.91 eV (Pb $4f_{7/2}$) and 143.74 eV (Pb $4f_{5/2}$) which confirms that the conjugated Pb^{2+}-aptamer has high specificity toward the Pb^{2+}. The results of Pb^{2+} detection in the Pb^{2+}-aptamer linked GOQD array sensor are shown in Fig. 3E-F. The F/F_0 of the GOQD array for Pb^{2+} sensor upon the on-chip processing of Pb^{2+} is shown in Fig. 3E. The F/F_0 value steadily decreased as increasing the Pb^{2+} concentration, which was also demonstrated in the FL scanning images of the quadruplicate GOQD array (inset of Fig. 3E). The semilog calibration curve in Fig. 3E shows high linearity in the range from 1 μM to 1 mM with the regression coefficient (R^2) of 0.986. Note that the linear response range of Cd^{2+} and Pb^{2+} concentration (1 μM to 1 mM) was shorter than that of As^{3+} (0.1 μM to 10 mM), which is attributed to the smaller number of unpaired electrons (two for Cd^{2+}, and four for Pb^{2+}, respectively) than that of As^{3+} (five). Indeed, charges on the quenchers (in this case, metal ions) could affect the extent of the quenching on the photoluminescent GOQD, which is a reason for different response range of the DNA-GOQD array sensor for As^{3+}, Cd^{2+}, and Pb^{2+}. The LOD value of the Pb^{2+} sensor is calculated as 4.44 nM, which is lower than U.S. EPA criterion for Pb^{2+} in drinking water (72.4 nM) (EPA, 2009). To evaluate the selective Pb^{2+} sensing ability of the GOQD array, we measured the F/F_0 values in the presence of other competitive metal ions (Concentration of all metal ions was 10 mM; As^{3+}, Cd^{2+}, Cu^{2+}, Hg^{2+}, Ag^{+}, and Fe^{3+}) under identical experimental conditions. As a NC, 10 mM of Pb^{2+} were processed on the pristine GOQD array without Pb^{2+}-aptamer (blue bar in Fig. 3F). As shown in Fig. 3F, most of the other competitive metal ions exhibit negligible interference. For a NC, higher F/F_0 value indicates that the conjugation of Pb^{2+}-aptamer on the GOQD array plays a key role for the specific binding of Pb^{2+}.

3.5. Multiplex metal ion detection on a chip

Benefiting from the successful monoplex heavy metal ion detection, we also investigated multiplex analysis on the integrated SPE-GOQD array microdevice (Fig. S6). For multiplex detection, we prepared a 6-spots of GOQD array on which the As^{3+}, Cd^{2+}, and Pb^{2+}-specific DNA aptamers were immobilized on two spots in parallel (Fig. S6A). After assembling the array sensor with the microdevice, a binary or ternary mixture of As^{3+} (5 mM), Cd^{2+} (0.5 mM), and Pb^{2+} (0.5 mM) aqueous solution was processed following the same on-chip procedure. When a As^{3+} and Cd^{2+} mixed solution was introduced, the FL of the As^{3+} and Cd^{2+}-aptamer linked GOQD array was significantly reduced (i of Figs. S6B and S6C) compared to that of the Pb^{2+}-aptamer linked GOQD array, which was also partially quenched. A simultaneous duplex detection of As^{3+} and Pb^{2+}, or Cd^{2+} and Pb^{2+} showed similar results (ii and iii of Figs. S6B and S6C). In case of the As^{3+}, Cd^{2+}, and Pb^{2+} mixed solution, all the FL signals of the GOQD array were clearly diminished with high efficiency (iv of Figs. S6B and S6C). These results suggest that an on-chip multiplex detection was successful with good distinguishability due to the highly specific response of the DNA-GOQD array sensor for targeting metal ions, although some interferences exist in the presence of multiple target metal ions (partial quenching (F/F_0 ~0.8) at the non-targeted GOQD array in the case from i to iii).

3.6. Measurement of metal ions in an environmental sample

Lake water was collected from Duck Lake in KAIST (Daejeon, Korea). The initial concentration of several metal ions was measured by an ICP-MS and a Direct Mercury Analyzer (DMA-80, Milestone Inc.) before spiking As^{3+}, Cd^{2+}, and Pb^{2+}. As shown in Table S3, metal ions were not detected except for Fe^{3+} (41 ppb) and Ni^{2+} (1 ppb), indicating that the Duck Lake water is suitable for real sample experiments. Certain amounts of As^{3+}, Cd^{2+}, and Pb^{2+} are spiked to the raw environmental sample, and the initial concentration of each metal ions was measured by ICP-MS or ICP-AES. Without any purification, an on-chip SPE based sample pretreatment was immediately performed, and the eluent was mixed with equimolecular NaOH solution in the outlet 1 for neutralization. The mixture was then automatically transferred to the GOQD array sensor unit by micropumping according to the operation process as described in 'On-chip metal ion detection on the photoluminescent GOQD array chip' section. Since the integrated microsystem provides rapid and automatic operation, the entire process from sample injection to detection could be completed within 45 min. The metal ion concentrations in a real sample measured by our microdevice were compared to the spiked values obtained from the ICP-based instruments. Table 1 shows the recovery of target metal ions in lake water within the range of 83–128% compared to the ICP-based method, which implies that our integrated SPE-GOQD array microdevice promises the practical applications of metal ion detection in an environmental sample.

4. Conclusions

In conclusion, we fabricated an integrated SPE-GOQD array microdevice for highly sensitive, selective, and multiplex detection of As^{3+}, Cd^{2+}, and Pb^{2+}. The on-chip SPE based sample pretreatment of As^{3+}, Cd^{2+}, and Pb^{2+} using cation exchange resins was successfully performed with high capture and release efficiency (> 80%). Then, the released As^{3+}, Cd^{2+}, and Pb^{2+} could be detected by the metal ion-specific DNA aptamer linked GOQD array sensor with detection limits of 5.03 nM, 41.1 nM, and 4.44 nM, respectively. Selection of the suitable cation exchange resin capable of adsorbing/desorbing more metal ions and the correspondent metal ion-specific DNA aptamer immobilized GOQD array will enable us to expand the multiplexing capability to detect more than three metal ions simultaneously.

Acknowledgements

This work was supported by the Engineering Research Center of Excellence Program of Korea Ministry of Science, ICT & Future Planning (MSIP)/National Research Foundation of Korea (NRF) (2014R1A5A1009799).

Appendix A. Supporting information

Supplementary data associated with this article can be found in the

online version at doi:10.1016/j.bios.2018.11.010.

References

Ananthanarayanan, A., Wang, X., Routh, P., Sana, B., Lim, S., Kim, D.H., Lim, K.H., Li, J., Chen, P., 2014. Adv. Funct. Mater. 24, 3021–3026.

Arpa, C., Bektas, S., 2006. Anal. Sci. 22, 1025–1029.

Au, A.K., Lai, H., Utela, B.R., Folch, A., 2011. Micromachines 2, 179–220.

Bell, J., Climent, E., Hecht, M., Buurman, M., Rurack, K., 2016. ACS Sens. 1, 334–338.

Bothra, S., Paira, P., Kumar SK, A., Kumar, R., Sahoo, S.K., 2017a. ChemistrySelect 2, 6023–6029.

Bothra, S., Upadhyay, Y., Kumar, R., Kumar, S.A., Sahoo, S.K., 2017b. Biosens. Bioelectron. 90, 329–335.

Camel, V., 2003. Spectrochim. Acta B Part B 58, 1177–1233.

Chen, B., Heng, S., Peng, H., Hu, B., Yu, X., Zhang, Z., Pang, D., Yue, X., Zhu, Y., 2010. J. Anal. At. Spectrom. 25, 1931–1938.

Choi, J.Y., Kim, Y.T., Byun, J.-Y., Ahn, J., Chung, S., Gweon, D.-G., Kim, M.-G., Seo, T.S., 2012. Lab Chip 12, 5146–5154.

Date, Y., Aota, A., Terakado, S., Sasaki, K., Matsumoto, N., Watanabe, Y., Matsue, T., Ohmura, N., 2012. Anal. Chem. 85, 434–440.

Daw, R., Finkelstein, J., 2006. Nature 442, 367.

EPA, 2009. National Primary Drinking Water Regulations. Publication No. EPA816-F-09-004 ed. Office of Water. U.S. Environmental Protection Agency (U.S. EPA), Washington, DC, USA.

Grover, W.H., Skelley, A.M., Liu, C.N., Lagally, E.T., Mathies, R.A., 2003. Sens. Actuators B 89, 315–323.

Ha, H.D., Jang, M.-H., Liu, F., Cho, Y.-H., Seo, T.S., 2015. Carbon 81, 367–375.

Helfferich, F.G., 1962. Ion Exchange Chromatography. McGraw-Hill.

Ibarlucea, B., Díez-Gil, C., Ratera, I., Veciana, J., Caballero, A., Zapata, F., Tárraga, A., Molina, P., Demming, S., Büttgenbach, S., 2013. Analyst 138, 839–844.

Jung, J.H., Cheon, D.S., Liu, F., Lee, K.B., Seo, T.S., 2010. Angew. Chem. Int. Ed. 122, 5844–5847.

Kim, H.N., Ren, W.X., Kim, J.S., Yoon, J., 2012a. Chem. Soc. Rev. 41, 3210–3244.

Kim, M., Um, H.-J., Bang, S., Lee, S.-H., Oh, S.-J., Han, J.-H., Kim, K.-W., Min, J., Kim, Y.-H., 2009. Environ. Sci. Technol. 43, 9335–9340.

Kim, Y.T., Chen, Y., Choi, J.Y., Kim, W.-J., Dae, H.-M., Jung, J., Seo, T.S., 2012b. Biosens. Bioelectron. 33, 88–94.

Kim, Y.T., Lee, D., Heo, H.Y., Sim, J.E., Woo, K.M., Im, S.G., Seo, T.S., 2016. Biosens. Bioelectron. 78, 489–496.

Lee, C.J., Jung, J.H., Seo, T.S., 2012. Anal. Chem. 84, 4928–4934.

Li, L., Wu, G., Yang, G., Peng, J., Zhao, J., Zhu, J.-J., 2013. Nanoscale 5, 4015–4039.

Li, S., Li, Y., Cao, J., Zhu, J., Fan, L., Li, X., 2014. Anal. Chem. 86, 10201–10207.

Li, T., Dong, S., Wang, E., 2010a. J. Am. Chem. Soc. 132, 13156–13157.

Li, T., Wang, E., Dong, S., 2010b. Anal. Chem. 82, 1515–1520.

Liu, F., Choi, J.Y., Seo, T.S., 2010. Biosens. Bioelectron. 25, 2361–2365.

Liu, F., Ha, H.D., Han, D.J., Seo, T.S., 2013. Small 9, 3410–3414.

Okamoto, I., Iwamoto, K., Watanabe, Y., Miyake, Y., Ono, A., 2009. Angew. Chem. Int. Ed. 48, 1648–1651.

Ono, A., Togashi, H., 2004. Angew. Chem. Int. Ed. 116, 4400–4402.

Park, M., Ha, H.D., Kim, Y.T., Jung, J.H., Kim, S.-H., Kim, D.H., Seo, T.S., 2015. Anal. Chem. 87, 10969–10975.

Shen, J., Zhu, Y., Yang, X., Li, C., 2012. Chem. Commun. 48, 3686–3699.

Sun, H., Wu, L., Wei, W., Qu, X., 2013. Mater. Today 16, 433–442.

Valeur, B., Leray, I., 2000. Coord. Chem. Rev. 205, 3–40.

Wang, F., Gu, Z., Lei, W., Wang, W., Xia, X., Hao, Q., 2014. Sens. Actuators B 190, 516–522.

Wu, Y., Zhan, S., Wang, F., He, L., Zhi, W., Zhou, P., 2012. Chem. Commun. 48, 4459–4461.

Wu, Y., Zhan, S., Wang, L., Zhou, P., 2014. Analyst 139, 1550–1561.

Zhao, L., Wu, T., Lefèvre, J.-P., Leray, I., Delaire, J.A., 2009. Lab Chip 9, 2818–2823.

Zheng, X.T., Ananthanarayanan, A., Luo, K.Q., Chen, P., 2015. Small 11, 1620–1636.

Zhu, X., Gao, C., Choi, J.-W., Bishop, P.L., Ahn, C.H., 2005. Lab Chip 5, 212–217.